RSC Advances

PAPER

View Article Online
View Journal | View Issue

Cite this: *RSC Adv.*, 2017, **7**, 23687

Corrosion inhibition of C-steel in acidic media from fruiting bodies of *Melia azedarach L* extract and a synergistic Ni^{2+} additive

A. I. Ali *[a] and Y. Sh. Mahrous[b]

The inhibiting ability of the fruiting bodies of *Melia azedarach Linn* extract (FB-MAL) and its synergistic effect with nickel ions (Ni^{2+}) on the corrosion of carbon (C)-steel in hydrochloric acid were investigated using gravimetric measurements, potentiodynamic polarization, and electrochemical impedance spectroscopy (EIS). The FB-MAL inhibited C-steel corrosion in acidic media up to 76.5%. Combining the FB-MAL with Ni^{2+} enhanced the adsorption capability of FB-MAL, greatly and consequently increased its inhibitive effect. Potentiodynamic polarization studies revealed that FB-MAL and FB-MAL + 100 ppm Ni^{2+} behave as mixed-type inhibitors. The EIS spectra showed that the charge transfer controls the corrosion process. The studied system obeys the Langmuir adsorption isotherm. The kinetic parameters were computed and are discussed later in this paper. The formation of the protective film was confirmed using Fourier transform-infrared spectroscopy, UV-Visible spectroscopy and scanning electron microscopy.

Received 5th January 2017
Accepted 14th April 2017

DOI: 10.1039/c7ra00111h

rsc.li/rsc-advances

1. Introduction

Iron or carbon (C)-steel alloys are widely used in many acidic industrial applications such as oil recovery, refining crude oil, and petrochemical processes. Such industries require many processes, *e.g.*, acid pickling, industrial cleaning, and acid descaling to be performed at regular intervals to improve the efficiency of the industrial process. Hydrochloric acid, phosphoric acid and/or sulfuric acids are widely preferred because of their regular aggressiveness as well as their special chemical properties.[1]

Corrosion is a ubiquitous problem that continues to be of great relevance in a wide range of industrial applications and products. It results in the degradation and eventual failure of components and systems both in the processing and manufacturing industries and in the service life of many components.

One of the most challenging and difficult tasks for industry is the protection of metals from corrosion. Corrosion damage can be prevented by using various methods such as upgrading materials used, blending of production fluids, process control and chemical inhibition.[2] Among these methods, the use of corrosion inhibitors is preferred as it prevents destruction or degradation of metal surfaces in corrosive media. The use of corrosion inhibitors is the most economical and practical method for reducing corrosive attack on metals. Corrosion inhibitors are either synthetic or natural chemicals, which when added in small amounts to an environment, decrease the rate of attack by the environment on the metals. However, in some cases the inhibitors used do not efficiently stop the corrosion. Increase in the effectiveness of a corrosion inhibitor can be accomplished using synergism. Synergism is when the combined effect of substances is greater than their individual effects. The synergistic effect is demonstrated in the presence of a secondary species, which can be a halide or a cation, depending on the type of the original inhibitor. Halide synergism[3] occurs because of the increased surface coverage achieved by the ion-pair interactions between the cationic organic inhibitor and the halide anion.

However, cations which have been used for synergism such as tin (Sn^{2+}) or copper (Cu^{2+}) mixed with a synthetic cationic gemini surfactant[4] to form a complex between the cations and the surfactant, have been shown to enhance the protection of the metal against corrosion.

A number of synthetic compounds[1,4] are known to be good corrosion inhibitors for metals. Nevertheless, the popularity and use of synthetic compounds as a corrosion inhibitor has diminished because of the strict environmental regulations and toxic effects of these compounds on human and animal life. Consequently, there exists a need to develop a new class of corrosion inhibitors with low toxicity, eco-friendliness and good efficiency.

The exploration of natural products as corrosion inhibitors is becoming the subject of extensive investigation, principally because of the low cost and eco-friendliness of these products.

[a]*Chemistry Department, Faculty of Science, Benha University, Benha 13512, Egypt. E-mail: drasmaa.ali10@yahoo.com; asmaa.ali@fsci.bu.edu.eg*

[b]*Central Metallurgical Research and Development Institute (CMRDI), Tebbin, PO Box 87, Helwan, Cairo 11421, Egypt. E-mail: mrous11@yahoo.com*

Plant extracts can be composed of several natural compounds which have corrosion inhibiting abilities. The yield of these compounds as well as the corrosion inhibition ability varies widely depending on the part of the plant[5] used and its location. The extracts from the leaves, seeds, heartwood, bark, roots and fruits of plants have been reported to inhibit metallic corrosion in acidic media.[5] Many plant extracts have been used as effective corrosion inhibitors of iron and steel in acidic media. Examples of these plants are: *Artemisia mesatlantica*,[6] *Murraya koenigii* leaf,[7] *strawberry fruit*,[8] *Medicago sativa*,[9] *Morinda tinctoria* leaves,[10] *Santolina chamaecyparissus*,[11] *Spirogyra* algae[12] and *Melia azedarach Linn* (MAL) seeds.[13] Most green corrosion inhibitors are obtained from methanol, ethanol, aqueous, acid, or formaldehyde extracts of plant materials.[14]

Melia azedarach Linn is a botanical species belonging to the family Meliaceae and it grows in many places around the world.[15] The phytochemical of the fruiting bodies of MAL (FB-MAL) contains active ingredients such as tannins and low molecular weight polyphenolic compounds. The major low molecular weight polyphenols identified are catechin and kaempferol which are flavonoids.[15] FB-MAL also contains water-soluble hetero-polysaccharides.[16] Furthermore, it contains oils such as palmitic, linolenic and linoleic acids.[17]

Contributing to the current interest on environmentally friendly corrosion inhibitors, the present study aims to broaden the application of plant extracts for metallic corrosion inhibition by investigating the inhibitive properties of aqueous FB-MAL on C-steel corrosion in 2 M HCl and to study the synergistic effect of FB-MAL + 100 ppm of nickel (Ni^{2+}). The degree of protection of FB-MAL, with and without 100 ppm of Ni^{2+}, against the corrosion of C-steel as well as the information about the mechanism of the inhibition process were determined using different techniques: potentiodynamic polarization, electrochemical impedance spectroscopy (EIS), gravimetric measurements, UV-Visible (UV-Vis) spectroscopy, Fourier transform-infrared (FT-IR) spectroscopy and scanning electron microscopy (SEM).

2. Experimental details

2.1 Materials

2.1.1 Preparation of plant extract. Fresh healthy fruiting bodies of MAL plants (FB-MAL) were dried at 318 K overnight. A portion (25 g) of the dried powdered plant sample was extracted with 250 mL of bi-distilled water. The sample was then refluxed at 333 K for 6 h. The solid FB-MAL residue was removed using filtration. The filtrate was evaporated to dryness at 353 K to obtain the plant extract to be used for further tests. FT-IR spectroscopy using a Nicolet iS 10 spectrophotometer was performed in the frequency range of 4000–400 cm^{-1} using the potassium bromide (KBr) pellet technique to identify the functional groups of the solid plant of FB-MAL.

2.1.2 Preparation of the specimens. The material used for constructing the working electrode was ASTM A573 Grade 70 low C-steel with a ASTM chemical composition (wt%) of: C 0.27%, Mn 0.85%, P 0.035%, S 0.035%, Si 0.15%, and the balance was Fe. The steel sheet was mechanically pressed to cut different coupons, which had a particular shape as described previously.[13] Rectangular C-steel specimens with dimensions of 1.2 cm × 1.1 cm × 0.75 cm were used for the gravimetric test. A C-steel cylinder, of the same composition, embedded in epoxy resin with an exposed area of 0.38 cm^2, was used as the working electrode (WE) for the potentiodynamic polarization and EIS measurements. The specimens were mechanically abraded with a series of emery papers of various grades, starting with a coarse one (600) and proceeding in steps to the finest (1000) grade. The sample was then washed thoroughly with bi-distilled water and degreased with acetone just before insertion in the cell.

2.1.3 Electrolyte. An aggressive solution of 2 M HCl was used as a corrosive medium and was prepared by diluting the concentrated acid (37% Merck) with bi-distilled water. A portion (1 g) of the solid FB-MAL was used to prepare a stock aqueous solution of 10 000 ppm in 100 mL of bi-distilled water. The desired concentrations of 50 ppm, 100 ppm, 200 ppm, 400 ppm, and 600 ppm were prepared by appropriate dilution and used for the corrosion inhibition activity tests. The co-inhibitor employed was 100 ppm of nickel chloride hexahydrate ($NiCl_2 \cdot 6H_2O$) which was prepared from an AR grade reagent.

2.2 Methods

2.2.1 Gravimetric measurements. Gravimetric measurements were carried out on C-steel coupons in 2 M HCl solution at various concentrations of FB-MAL with and without 100 ppm of Ni^{2+} for 6 h at 303 K in naturally aerated solutions as described previously.[13]

The corrosion rate was calculated in milligrams per square centimeter per hour (mg cm^{-2} h^{-1}) using the following equation:

$$CR_w = \frac{W}{S \times t} \quad (1)$$

where W is the average loss in weight (mg), S is the surface area (cm^{-2}) of the worked specimen and t is the exposure time (h).

The inhibition efficiencies (IE) were evaluated using to eqn (2), where CR_W^0 and CR_W are the corrosion rates without and with the inhibitor, respectively.

$$IE_{(w)} = \frac{CR_{W^0} - CR_W}{CR_{W^0}} \times 100 \quad (2)$$

The degree of surface coverage of the inhibitor molecules at the metal surface were determined from $IE_{(W)}$ using the following equation:

$$\theta = \frac{CR_{W^0} - CR_W}{CR_{W^0}} \quad (3)$$

2.2.2 Electrochemical experiments. Electrochemical experiments were performed in a 50 mL borosilicate glass cell using platinum wire and a saturated calomel electrode (SCE) as auxiliary and reference electrodes, respectively. The SCE was connected *via* a Luggin capillary, the tip of which was very close to the surface of the WE to minimize the voltage (*IR*) drop. The electrochemical experiments were carried out in the media

being studied after attaining the open circuit potential (E_{ocp}). Potentiodynamic polarization measurements were carried out in the direction from the cathode to the anode at a scan rate of 10 mV s^{-1}.[18,19] A Meinsberger potentiostat/galvanostat with PS6 software was used for the polarization measurements.

The IE and fractions of surface coverage (θ) were evaluated from following equations:

$$IE = \left[1 - \left(\frac{i_{corr}}{i^0_{corr}}\right)\right] \times 100 \quad (4)$$

$$\theta = 1 - \left(\frac{i_{corr}}{i^0_{corr}}\right) \quad (5)$$

where i^0_{corr} and i_{corr} are the corrosion current density of the steel specimen (mA cm^{-2}) for the uninhibited and inhibited solutions, respectively.

EIS experiments were conducted using a computer controlled Princeton Applied Research PARSTAT 4000 teamed with the VersaStudio software package for calculation of corrosion parameters such as charge transfer resistance (R_{ct}) and some parameters related to double layer capacitance (C_{dl}) values. EIS studies were carried out at a potential amplitude of 10 mV, peak to peak (AC signal) in the frequency ranging from 100 kHz to 0.1 Hz.

The IE of FB-MAL and FB-MAL + 100 ppm Ni^{2+} treated C-steel alloy were computed using the following equation:

$$IE = \left[1 - \left(\frac{R_{ct(0)}}{R_{ct(i)}}\right) \times 100\right] \quad (6)$$

where $R_{ct(0)}$ and $R_{ct(i)}$ are the charge transfer resistance of C-steel for uninhibited and inhibited solutions, respectively.

2.3 Scanning electron microscopy (SEM)

The surface morphology of C-steel specimens immersed in 2 M HCl, 2 M HCl + 600 ppm FB-MAL, and 2 M HCl + 600 ppm FB-MAL + 100 ppm Ni^{2+}, respectively, were studied using a FEI Quanta FEC 250 SEM microscope. The specimens were immersed in the test solutions for 6 h before analysis at 303 K. SEM images of the C-steel coupons were compared using different experimental conditions.

2.4 UV-Visible spectroscopy

The adsorption behavior of the organic compounds of FB-MAL at the C-steel surface with and without 100 ppm Ni^{2+} were confirmed using UV-Vis spectroscopy. The analyses were performed on Jasco V-530 UV-Vis spectrophotometer within the range 200 nm to 1300 nm using a 10 mm matched silica cell. A 50 ppm FB-MAL solution in 2 M HCl as a control was analyzed before and after the weight loss tests (with and without 100 ppm of Ni^{2+}). The test spectra obtained were compared with the control to investigate its adsorptive nature.

2.5 FT-IR spectroscopy

The nature of the surface film formed at the C-steel electrode in 2 M HCl solution in the presence of FB-MAL with and without 100 ppm Ni^{2+} cations were examined by collecting the layers produced after the weight loss test by scratching the C-steel coupons, washing them carefully with bi-distilled water and then analyzing them using FT-IR spectroscopy.

3. Results and discussion

3.1 FT-IR spectroscopy of FB-MAL

Fig. 1 shows the FT-IR spectra for FB-MAL. It can be seen from the figure, that –OH stretching bands of alcohol or phenol can be assigned at 3418.75 cm^{-1}. The band at 2936 cm^{-1} is related to the –C–H aromatic stretching frequency. The –C=C– vibrations in aromatic rings or alkenes are assigned at 1633 cm^{-1}. The assigned band at 1412.44 cm^{-1} corresponds to the $-CH_2$ bending frequency. Vibration of the aromatic ring appears at 1256 cm^{-1}. The band that appeared at 1079 cm^{-1} is associated with –C–O stretching vibration. A series of absorption bands below 1000 cm^{-1} are ascribed to aliphatic and aromatic C–H group vibrations. Therefore, it was concluded that, FB-MAL contains aromatic rings and different oxygenated functional groups, which meet the standard specification of inhibitors. Fig. 2 shows the chemical composition of the major constituents of extract tested[15–17] which agrees with the FT-IR results.

3.2 Gravimetric measurements

3.2.1 Effect of concentration. The weight loss method of monitoring the corrosion inhibition is useful because of its simple application and good reliability. In the present study, the experimental reproducibility of both corrosion rate and IE in a triplicate determination is good (the relative standard deviation values of three parallel experiments were lower than 2% as shown in Table 1).

The corrosion rate values, degree of surface coverage (θ), and the IE in 2 M HCl contain different concentrations of FB-MAL with and without 100 ppm Ni^{2+} at 303 K are listed in Table 1. It is seen from the results in Table 1 that increasing the FB-MAL concentration decreases the corrosion rate of C-steel, consequently increasing both θ and IE. This behavior could be related to the increase in adsorption of FB-MAL molecules at the metal/solution interface with increasing concentration. The results in

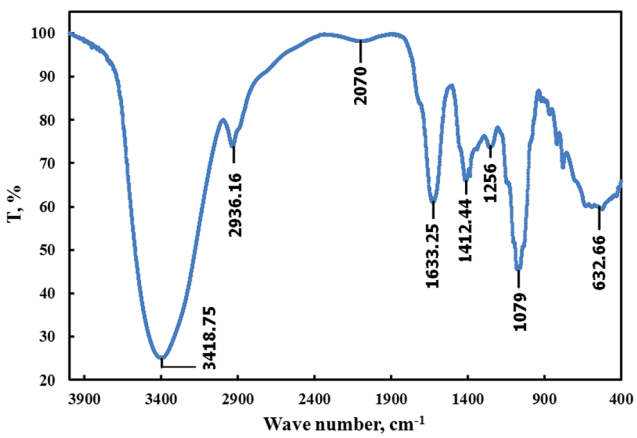

Fig. 1 FT-IR for FB-MAL.

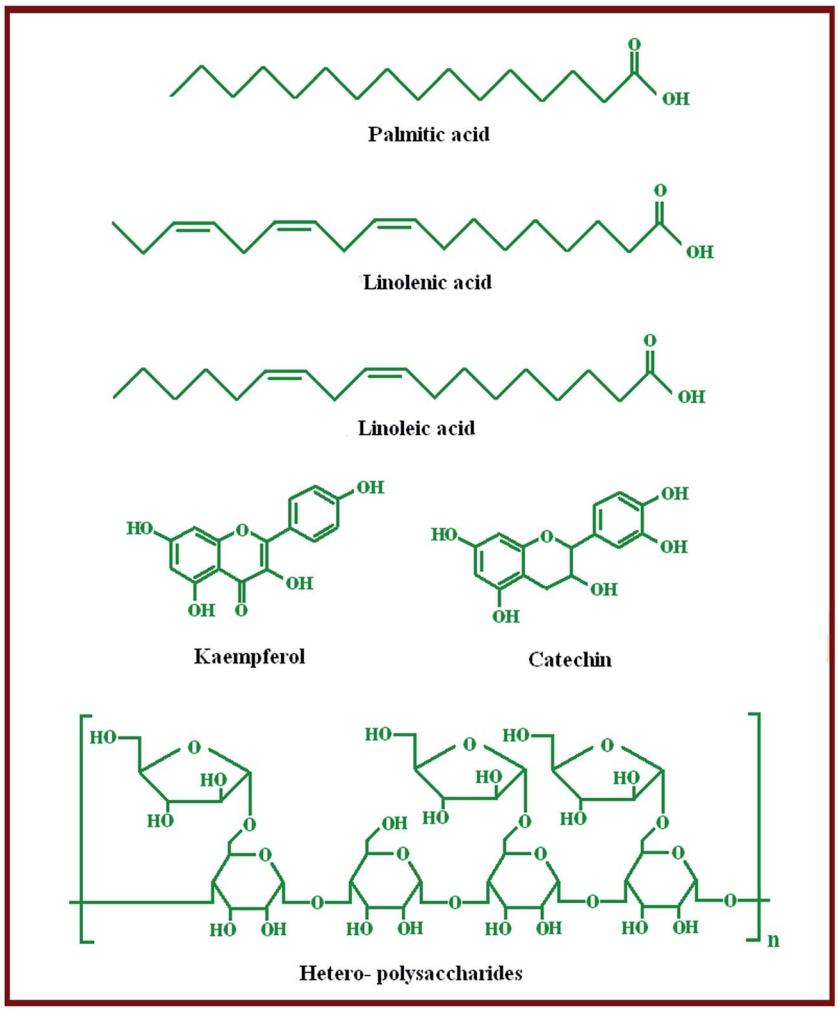

Fig. 2 Chemical structures of the major components of FB-MAL.

Table 1 Corrosion rate, degree of surface coverage and corrosion IE of FB-MAL with and without 100 ppm Ni^{2+} for C-steel in 2 M HCl at 303 K

C_{cation} (ppm)	FB-MAL concentration (ppm)	Corrosion rate (mg cm^{-2} h^{-1})	Surface coverage (θ)	IE (%)
0	0	3.500 ± 0.13	—	—
	50	2.800 ± 0.92	0.200	20.00 ± 1.54
	200	1.954 ± 0.72	0.442	44.00 ± 1.09
	400	1.297 ± 0.62	0.629	62.95 ± 0.91
	600	0.821 ± 0.52	0.765	76.56 ± 0.91
100 ppm Ni^{2+}	50	2.040 ± 0.85	0.417	41.68 ± 1.23
	200	1.330 ± 0.79	0.620	62.01 ± 1.17
	400	0.706 ± 0.78	0.798	79.83 ± 1.22
	600	0.250 ± 0.52	0.929	92.86 ± 0.80

Table 1 also show that addition of 100 ppm Ni^{2+} to different concentrations of FB-MAL in a corrosive media effectively decreases the C-steel corrosion rate. These results indicate that this synergistic system can effectively be adsorbed at the low C-steel surface forming a protective layer, which prevents diffusion of the corrosive medium and hindering its destructive effect. The effect of FB-MAL at different concentrations on the IE (%) of C-steel immersed in 2 M HCl with and without 100 ppm Ni^{2+} are shown in Fig. 3. In the absence of the metal cation, the IE shows a small inhibitive effect even with an increased concentration of the FB-MAL. The maximum IE of 76.5% was attained using 600 ppm of the extract, and further increase in the concentration did not cause any significant change in the inhibitor performance. This finding was attributed to several factors: (1) the saturation state of the molecules adsorbed at the C-steel surface, and (2) steric effects operating

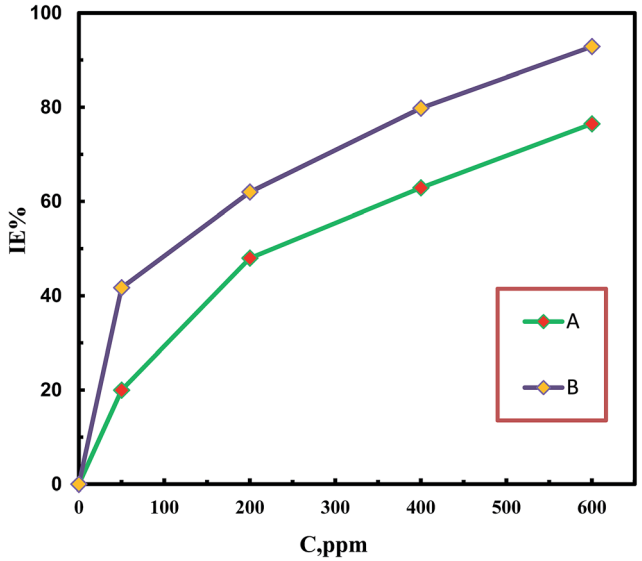

Fig. 3 Relationship of the IE of C-steel in 2 M HCl after 6 h immersion time as a function of FB-MAL concentrations (A) and FB-MAL concentrations + 100 ppm of Ni^{2+} (B).

between these adsorbed particles. However, at all concentrations of FB-MAL studied, the presence of 100 ppm of Ni^{2+} enhanced the inhibition performance of the extract because of the increased surface coverage given by FB-MAL and Ni^{2+}. These results suggest that there is a synergistic effect between FB-MAL molecules and Ni^{2+} ions. The inhibition efficiency was raised to approximately 93% by addition of 100 ppm of Ni^{2+} ions to aggressive media containing 600 ppm of FB-MAL.

3.2.2 Kinetic parameters of the corrosion process. Gravimetric measurements were performed in 2 M HCl, 2 M HCl + 600 ppm FB-MAL, and 2 M HCl + 600 ppm FB-MAL + 100 ppm Ni^{2+} solutions. The experiments were performed at a temperature range from 303 K up to 343 K for 6 h. Fig. 4 shows the relationship between the corrosion rate and temperature in both free and inhibited solutions. It is obvious that, the corrosion rate increases with increasing temperature for the systems studied. But the corrosion rate increases more rapidly without the inhibitors studied compared to with them. This was attributed to high dissolution of the metal with temperature rise, which enhanced the corrosion rate. Also, increasing the corrosion rate with temperature in the presence of the inhibitors studied can be attributed to a decrease in the adsorption capacity of the inhibitor molecules at the C-steel surface because of the increase in the desorption rate.

The synchronous presence of 100 ppm of Ni^{2+} with 600 ppm FB-MAL in the corrosive media effectively retarded the corrosion rate of C-steel (compared to 600 ppm FB-MAL alone) as a result of a protective film formed at the metal surface.

The dependence of the corrosion rate on temperature can be expressed using Arrhenius equation:[18]

$$\log CR = \log A - \left(\frac{E_a}{2.303RT}\right) \quad (7)$$

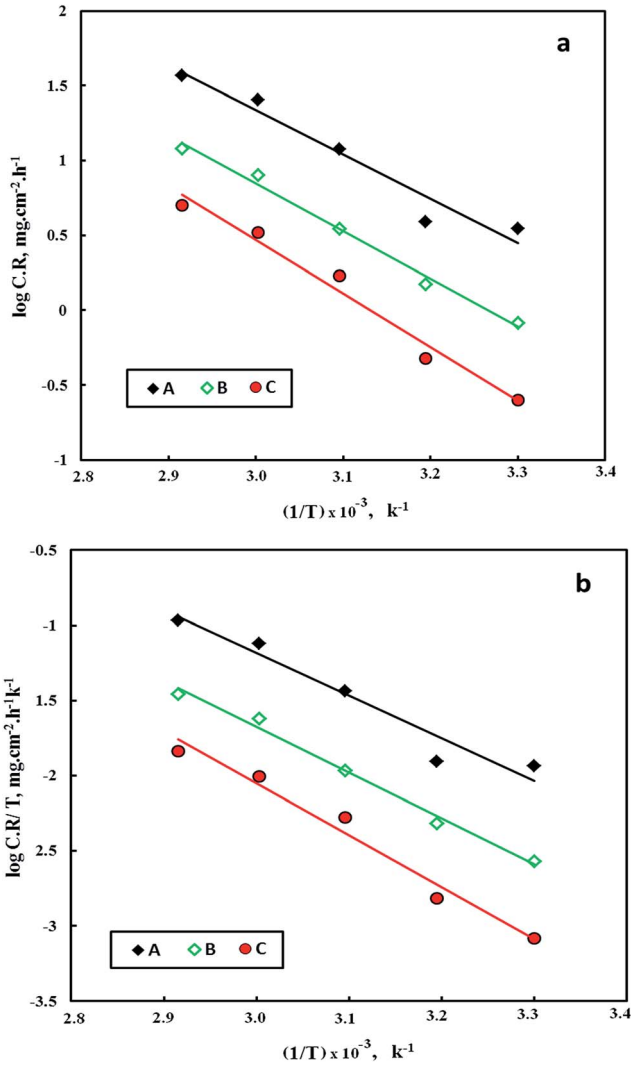

Fig. 4 Arrhenius (a) and alternative Arrhenius (b) plots for C-steel in: 2 M HCl (A), 2 M HCl + 600 ppm FB-MAL (B), 2 M HCl + 600 ppm FB-MAL + 100 ppm Ni^{2+} (C).

The apparent activation energies (E_a) for the corrosion process were calculated using the plots in Fig. 4a and are given in Table 2. It is obvious that the presence of FB-MAL or FB-MAL in synergy with Ni^{2+} increases the apparent E_a compared to the blank value. This result is generally interpreted as a strong adsorption of different inhibitors at the C-steel surface.[3,20]

The thermodynamic parameters for corrosion of C-steel in free 2 M HCl solution, and that containing 600 ppm of FB-MAL in both with and without 100 ppm Ni^{2+} were calculated from the slopes and intercepts of lines in Fig. 4b using the following equation:[20]

$$\log\frac{CR}{T} = \left[\left(\frac{R}{Nh}\right)\right] + \left[\left(\frac{\Delta S^*}{2.303R}\right)\right] - \left(\frac{\Delta H^*}{2.303RT}\right), \quad (8)$$

where N is the Avogadro number, h is Planck constant, and ΔS^*, and ΔH^*, are the entropy, and enthalpy of activation of the corrosion process, respectively.

Table 2 Activation parameters of the dissolution of C-steel in 2 M HCl with and without 600 ppm FB-MAL in with and without 100 ppm of Ni^{2+}

Activation parameters	ΔE_a^* (kJ mol^{-1})	ΔH^* (kJ mol^{-1})	ΔS^* (kJ mol^{-1} K^{-1})
2 M HCl	64.66	61.96	−0.343
2 M HCl + fruiting body extract	68.09	65.38	−0.334
2 M HCl + fruiting body extract + Ni^{2+}	76.52	73.82	−0.157

The values of ΔS^* and ΔH^* were calculated and are given in Table 2. The data in Table 2 revealed that the inhibited solutions showed high values of ΔH^* compared to that obtained for the uninhibited one indicating a higher protection efficiency.[20] The adsorption process leads to a rise in the enthalpy of activation through the increase in the energy barrier for the dissolution reaction, thus, slowing the dissolution of C-steel in the presence of inhibitors. The positive values of ΔH^* reflect the endothermic nature of the dissolution of the tested alloy in the corrosive media. The low negative values of the entropy of activation in the presence of the inhibitors compared to the free acid solution, suggest that there is an increase in randomness which occurred while moving from reactants to the activated complex.[20]

3.3 Potentiodynamic polarization

3.3.1 Effect of concentration. Fig. 5 shows the potentiodynamic polarization measurements for C-steel in 2 M HCl at different concentrations of FB-MAL. Both the anodic and cathodic branches of the polarization curves display Tafel behavior. It is clear that the presence of FB-MAL causes a marked decrease in the corrosion rate where both the cathodic and anodic branches of the Tafel plot shift to a lower current density at all investigated concentrations.

Measurements of potentiodynamic polarization were also carried out for C-steel in 2 M HCl solution containing different concentrations of FB-MAL in the presence of 100 ppm of Ni^{2+} (not shown). The values of the electrochemical kinetic parameters: corrosion potential (E_{corr}), corrosion current density (i_{corr}) and Tafel slope constants (β_a and β_c), were determined using the well known Tafel extrapolation method, and the results are summarized as a function of inhibitor concentration in Table 3. It is clear that in the systems tested, that increasing inhibitor concentration decreases i_{corr}, β_a, and β_c whereas E_{corr} does not change significantly. This indicates that the inhibitors tested behave as mixed type inhibitor, where they are adsorbed at the alloy surface and then impeded the electrochemical reaction by merely blocking the reaction sites of the alloy surface without affecting the anodic and cathodic reaction (this does not change the mechanism of iron dissolution and hydrogen evolution reactions).

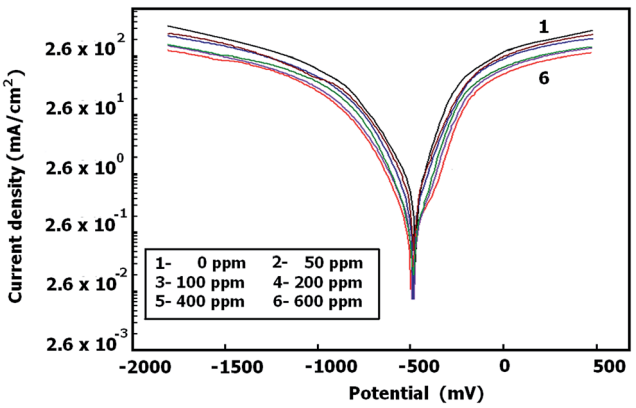

Fig. 5 Tafel plots for C-steel in 2 M HCl containing different concentrations of FB-MAL.

Table 3 shows that the presence of 100 ppm of Ni^{2+} gives a slight increase of the corrosion inhibition of C-steel alloy in free HCl. This result can be attributed to the inorganic cathodic inhibitor nature of the Ni^{2+} cations because of its alkalinity.[21–24] The corrosion inhibition by Ni^{2+} may be because its adsorption at the cathodic reaction sites helps to form a compact and adherent film that restricts the diffusion of reducible species, thus decreasing the main cathodic reaction[21] demonstrated by the following equation:

$$2H^+ + 2e \rightarrow H_2\uparrow \quad (I)$$

Therefore, the corrosion reaction is hindered because of the blocking of the reaction path of the iron dissolution.

It is obvious from results in Table 3 that the presence of 100 ppm of Ni^{2+} at different concentrations of FB-MAL causes a marked decrease in the corrosion rate (i_{corr}) (compared to FB-MAL alone), consequently, the IE increases significantly. These results indicate that the addition of 100 ppm of Ni^{2+} at different concentrations of FB-MAL increases the surface coverage by the different adsorbed molecules of FB-MAL and consequently decreases the reaction rate. This result means that FB-MAL acts efficiently as a corrosion inhibitor for C-steel protection in the presence of 100 ppm of Ni^{2+} because of the synergistic effect.

3.3.2 Synergism. The inhibiting effect of organic inhibitors is mainly related to their adsorption behavior at the metal surface, which depends on the molecular structure of the compounds tested and the surface charge density and the potential of zero charge of the metal.

This interaction can be increased by synergism. The synergism parameter (S_θ) is defined as:[3,25]

$$S_\theta = \frac{1-\theta_{1+2}}{1-\theta'_{1+2}} \quad (9)$$

where $\theta_{1+2} = (\theta_1 + \theta_2) - \theta_1\theta_2$, θ_1 and θ_2 are the degrees of surface coverage in the presence of different concentrations of FB-MAL, and 100 ppm of Ni^{2+}, individually. Where θ'_{1+2} is the degree of surface coverage in the presence of both species.

Table 3 Electrochemical and synergism parameters of C-steel in 2 M HCl with and without different concentrations of FB-MAL with and without 100 ppm of Ni^{2+}

System	C_{MAL} (ppm)	E_{corr} (mV)	i_{corr} (mA cm^{-2})	β_a (mV dec^{-1})	β_c (mV dec^{-1})	IE (%)	S_θ
2 M HCl	0	−480	1.35	174	−228	—	—
2 M HCl + 100 ppm Ni^{2+}	0	−464	0.66	149	−209	51.11	—
2 M HCl	50	−437	1.02	140	−209	24.44	—
	100	−452	0.883	130	−185	34.59	—
	200	−437	0.630	101	−164	53.33	—
	400	−458	0.350	107	−143	74.07	—
	600	−465	0.338	100	−140	74.96	—
2 M HCl + 100 ppm Ni^{2+}	50	−438	0.430	100	−170	68.14	1.16
	100	−440	0.38	98	−174	71.85	1.14
	200	−451	0.24	100	−155	82.22	1.28
	400	−430	0.17	97	−189	87.41	1.03
	600	−427	0.093	83	−160	93.11	1.74

S_θ approaches unity when no interaction takes place between the inhibitor molecules and the cation tested. At $S_\theta > 1$, a synergistic effect is obtained which is a result of co-operative adsorption. For $S_\theta < 1$, antagonistic behavior prevails because of competitive adsorption.[3] Table 3 shows the S_θ estimated for C-steel in 2 M HCl solution containing 100 ppm of Ni^{2+} and different concentrations of FB-MAL. The S_θ values were found to be more than unity, suggesting a co-operative adsorption of Ni^{2+} with the FB-MAL. These results indicate that the FB-MAL can act as an effective inhibitor for C-steel in a 2 M HCl solution even at a low concentration in the presence of 100 ppm Ni^{2+} because of the synergistic effect.

3.3.3 Adsorption isotherm. Organic compounds show their inhibitive effect because of the formation, by adsorption, of a protective film at the metal surface. The adsorption process occurs by replacing the water molecules at the metal interface by the inhibitor molecules according to following equation:

$$Org_{(sol)} + nH_2O_{(ads)} \rightarrow Org_{(ads)} + nH_2O_{(sol)} \quad (II)$$

where both $Org_{(sol)}$ and $Org_{(ads)}$ are the inhibitor molecules in the aggressive media and which were adsorbed at the metal surface, and n is the number of water molecules replaced by the organic inhibitor molecules.

The interaction between the metal and the inhibitor molecules can be described by different adsorption isotherms.[26,27] From the experimental results, it was found that a correlation between surface coverage (θ) and the concentration (C) of inhibitors in the aggressive media was represented by the Langmuir adsorption isotherm according to the following equation:

$$\frac{C_{inh}}{\theta} = \frac{1}{K_{ads}} + C_{inh} \quad (10)$$

and

$$K_{ads} = \frac{1}{C_{solvent}} \exp\left(-\frac{\Delta G^\circ_{ads}}{RT}\right) \quad (11)$$

where R is the gas constant (8.314 J mol K^{-1}), T the absolute temperature (K), ΔG°_{ads} is the standard free energy of adsorption and $C_{solvent}$ is the concentration of water in solution which has the value 1.106 mg L^{-1}. The θ values were computed from potentiodynamic plots at 303 K (by using eqn (5)).

Plotting C_{inh}/θ *versus* C_{inh} resulted in straight lines as shown in Fig. 6, where both the linear correlation coefficient (R^2) and the slopes are very close to unity, indicating that the adsorption of the FB-MAL and Ni^{2+} FB-MAL species at the C-steel surface obey the Langmuir adsorption isotherm in the 2 M HCl solution. According to the Langmuir adsorption isotherm, the inhibitor molecules tested have a typical adsorption site at the metal/solution interface with no interaction with the other molecules adsorbed.[28]

The adsorption equilibrium constant (K_{ads}) for both FB-MAL, FB-MAL + 100 ppm Ni^{2+}, can be calculated using the reciprocal of the intercept of the $C_{inh}/\theta - C_{inh}$ curve. The values of K_{ads} for FB-MAL, and FB-MAL + 100 ppm Ni^{2+} were 0.006 and 0.023 M^{-1}, respectively. The value of K_{ads} for FB-MAL + 100 ppm Ni^{2+} was greater than that for FB-MAL alone. This result can be interpreted as the adsorption of FB-MAL in presence of Ni^{2+} was more efficient because of the increasing capability of adsorption

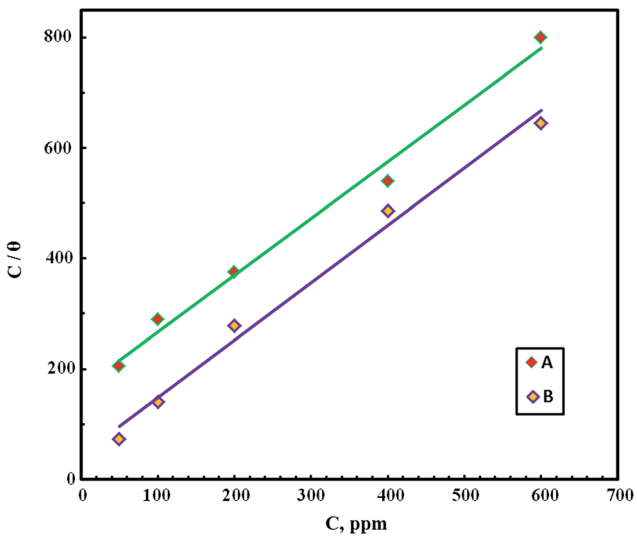

Fig. 6 Langmuir adsorption isotherm for FB-MAL concentrations (A), FB-MAL concentrations + 100 ppm of Ni^{2+} (B).

at the metal surface and thus, the inhibition efficiency was improved.[3,29] K_{ads} is related to ΔG°_{ads} according to eqn (11). The calculated values of ΔG°_{ads} obtained for FB-MAL, and FB-MAL + 100 ppm Ni^{2+} were −21.7, and −24.94 kJ mol^{-1}, respectively, indicating that the adsorption mechanism of the inhibitors at the C-steel in 2 M HCl solution involved electrostatic adsorption.[8,12] The calculated values of ΔG°_{ads}, indicated that both physisorption (major contributor) and chemisorption (minor contributor) of the inhibitors occur at the metal surface. It is obvious that the calculated ΔG°_{ads} values in the presence of Ni^{2+} with FB-MAL were more negative than that in its absence. This suggests that there is the formation of a strong adsorbed film in the presence of Ni^{2+} with FB-MAL at the C-steel surface.

3.4 Electrochemical impedance spectroscopy (EIS)

Fig. 7a–c shows the Nyquist (a), Bode (b) and Bode phase (c) plots obtained for C-steel sample in 2 M HCl solution containing different concentrations of FB-MAL. Measurements of EIS were also conducted for C-steel in 2 M HCl solution containing 600 ppm of FB-MAL in presence of 100 ppm of Ni^{2+} (results not shown). Inspection of Fig. 7a reveals that the Nyquist plot of C-steel in 2 M HCl containing different concentrations of FB-MAL does not give the typical semicircle which is according to EIS theory. The variation from ideal semicircle is assigned to the frequency dispersion, the inhomogeneities of the C-steel surface and the mass transport resistance.[30] The depressed Nyquist plot referring to C-steel corrosion in 2 M HCl solution is predominately determined by a charge transfer process.[30] The diameter of the semicircles (or the value of charge transfer resistance, R_{ct}) of C-steel specimens in the Nyquist plot was considerably increased with increasing concentrations of FB-MAL (Fig. 7a). The increase of the semicircle diameter in the Nyquist plot revealed that the FB-MAL shows good efficiency in corrosion control of C-steel, which could be associated with the significant adsorption of FB-MAL components at the C-steel surface in the pickling solution.[31–33] An increase in charge transfer resistance could increase the tendency of the current to pass through the capacitor in the circuit leading to the capacitive behavior of the electrode/electrolyte system.[31] Similar behavior of the Nyquist plot was obtained when 600 ppm of FB-MAL + 100 ppm of Ni^{2+} were used.

The experimental α value, which determined the alloy surface irregularity, were calculated from the slope of the linear region of log(*f*) *versus* log|*Z*| plots (Fig. 7b) and results given in Table 4. Theoretically, the value of α should be equal to −1 for an ideal capacitor. It was found that the α-values for C-steel in the corrosive media studied (with and without inhibitors) were less than 1. This result was attributed to the corrosion of the steel in 2 M HCl solution leading to coarseness of the metal surface, and thus, heterogeneity of the C-steel surface was attained. It can be seen from Table 4, that the presence of FB-MAL or 600 ppm of FB-MAL + 100 ppm Ni^{2+}, both in 2 M HCl solution increased the α-value from −0.57 to −0.95, thus indicating the decrease of heterogeneity of the metal surface as a result of adsorption of the two inhibitors studied. Fig. 7c shows that increasing the concentration of FB-MAL in 2 M HCl

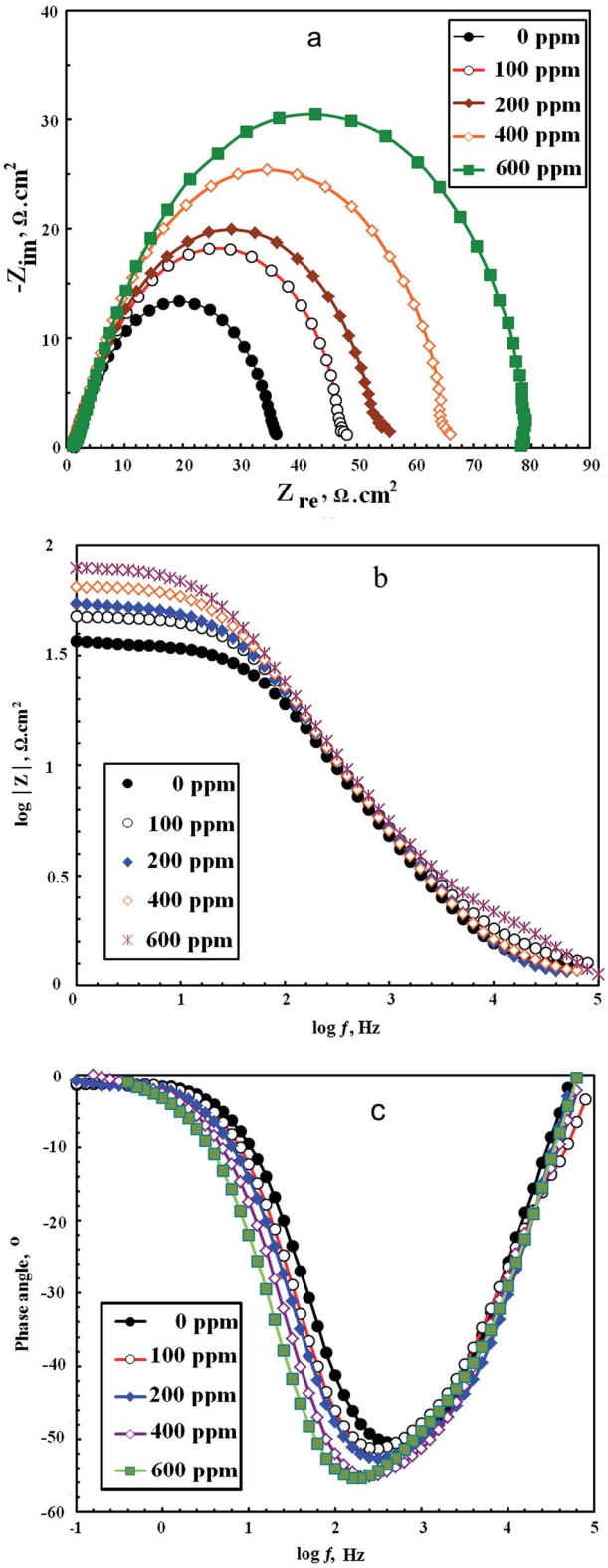

Fig. 7 Nyquist (a) Bode (b) and Bode phase (c) plots of a C-steel electrode in 2 M HCl solution with and without different concentrations of FB-MAL.

results in more negative values of phase angle indicating that the inhibitive behavior occurred because more of the FB-MAL molecules adsorbed at the C-steel surface forming a FB-MAL

Table 4 EIS parameters of C-steel in 2 M HCl with and without different concentrations of FB-MAL with and without 100 ppm Ni^{2+}

C_{MAL} (ppm)	C_{cation} (ppm)	R_s (Ω cm^2)	R_{ct} (Ω cm^2)	Q (s^{α} Ω^{-1} cm^{-2})	f_{max} (Hz)	α	IE (%)
0	0	1.68	34.85	0.027	63.10	−0.57	—
100	0	1.50	45.70	0.021	50.11	−0.60	23.74
200	0	1.64	52.00	0.018	39.80	−0.61	32.98
400	0	1.90	64.10	0.015	25.12	−0.63	45.63
600	0	1.66	77.00	0.013	19.95	−0.64	54.74
600	100 ppm Ni^{2+}	1.02	245.11	5.9×10^{-5}	12.00	−0.95	85.78

complex which was able to protect the surface of C-steel from corrosion and thus giving rise to a low corrosion rate. It is seen from the Nyquist and Bode plots, one semicircle and a single peak, respectively. These results indicated the existence of one time constant in the electrochemical process related to the electrical double layer formed at the C-steel surface-solution interface.

Nyquist plots simulate Randles' model because the experimental data agree with it as shown in Fig. 8. R_s denotes the solution resistance, R_{ct} is the Nyquist plot diameter which is expressed by the charge transfer resistance and CPE is the constant phase element which replaces the capacitance of the electrical double layer (C_{dl}).[30]

The impedance of the CPE is expressed by the following equation:[33,34]

$$Z_{CPE} = Q^{-1}(J\omega)^{-\alpha}, \quad (12)$$

where Q is a proportional factor (s^{α} Ω^{-1} cm^{-2}), $j^2 = -1$ is an imaginary number, and ω is the angular frequency in rad^{-1}.

Table 4 shows the corrosion parameters obtained from EIS plots. Inspection of Table 4 reveals that the values of R_{ct} are increased with increase in the FB-MAL concentration and this occurs as a result of adsorption of the inhibitor molecules at the C-steel surface forming a protective layer which can isolate the metal surface from the aggressive media, and consequently, the IE_{EIS} increased with increasing FB-MAL concentration. However, the presence of 100 ppm of Ni^{2+} with 600 ppm of FB-MAL increases the R_{ct} sufficiently and consequently there is an efficient increase in IE_{EIS}. Also it can be seen from the results in Table 4 that the Q_{dl} values decreased with increasing FB-MAL concentration and this may be because of the increment of electrical double layer thickness because of the adsorbed molecules of the extract on metal surface and replacement of water molecules by FB-MAL molecules. However, the presence of 600 ppm FB-MAL + 100 ppm of Ni^{2+} in the corrosive solution decreases Q_{dl} sufficiently. The increase of the "α" parameter with increasing concentration of the extract could be related to the adsorption of inhibitor molecules at the metal surface which lead to less heterogeneity of the C-steel surface. At 600 ppm of FB-MAL with and without 100 ppm of Ni^{2+}, the "α" value changed from −0.64 to −0.95, indicating an efficient reduction of surface heterogeneity in presence of Ni^{2+}. This behavior secures the synergistic effect of Ni^{2+} with FB-MAL molecules because of the formation of a protective film or complex from the acidic solution at the metal/solution interface.[34]

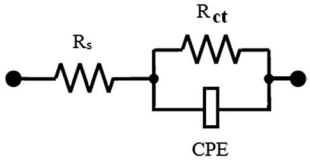

Fig. 8 The electrochemical equivalent circuit used to fit the impedance spectra.

3.5 Inhibition mechanism

FB-MAL is an oxygen-containing organic compound (see Section 3.1), which contains lone-pair electrons and π-electrons. The FB-MAL constituents exist either as neutral molecules or protonated molecules in HCl solution as follows:

$$\text{FB-MAL} + x\text{H}^+ \leftrightarrow [\text{FB-MALH}_x]^{x+} \quad \text{(III)}$$

In addition, the potential of zero charge ($E_q = 0$) for iron in HCl is −590 mV *versus* SCE. In the present case, E_{corr} equals −480 mV *versus* SCE of C-steel in 2 M HCl solution. Consequently, the C-steel surface carries a positive charge because of the $E_{corr} - E_q = 0 > 0$.[35,36] Therefore, FB-MAL may be adsorbed at the C-steel/acid solution interface by one or more of the following ways:

(i) The protonated organic compounds of FB-MAL may be adsorbed through its electrostatic interactions with the positively charged metal surface by using chloride ions attached to the metal surface as a negative bridge. Afterwards the donor–acceptor interaction is achieved between the oxygen atom or π-electrons of FB-MAL constituents and the vacant d-orbital of the surface iron atoms (or may be linked with the freshly generated Fe^{2+} ions at the steel surface) forming metal inhibitor complexes as follows:

$$\text{Fe} \rightarrow \text{Fe}^{2+} + 2\text{e}^- \quad \text{(IV)}$$

$$[\text{FB-MALH}_x]^{x+} + \text{Fe}^{2+} \rightarrow [\text{FB-MALH}_x\text{-Fe}]^{(2+x)+} \quad \text{(V)}$$

(ii) The neutral organic compounds of FB-MAL may be adsorbed at the metal surface *via* the chemisorption mechanism, involving the displacement of water molecules from the metal surface, where the FB-MAL molecules can be adsorbed at the metal surface on the basis of donor–acceptor interactions between π-electrons and/or oxygen and vacant d-orbitals of Fe.[6] Interaction between unshared electron pairs of oxygen or

π-electrons of the aromatic ring of FB-MAL molecules and vacant d-orbital of surface iron atoms is as follows:

$$Fe{\cdot}H_2O_{ads} + \text{FB-MAL} \rightarrow Fe{\cdot}\text{FB-MAL}_{ads} + H_2O \qquad \text{(VI)}$$

(iii) In this present research, the presence of 100 ppm of Ni^{2+} in inhibited solutions increase the surface coverage of the C-steel. These results can be explained because of Ni^{2+}, which as a transition element has a vacant orbit (3d). However, on the other side FB-MAL contains oxygen atoms with a lone pair of electrons and π-electrons of the aromatic rings. When the extract and Ni^{2+} were mixed, the new complex Ni^{2+} FB-MAL was easily produced. This complex plays an important role in the enhancement of the protection of C-steel against corrosion.[4] Stabilization of adsorbed Ni^{2+} with FB-MAL lead to greater surface coverage at the C-steel surface and thereby greater inhibition efficiency. The complex is able to be adsorbed at the steel surface because of van der Waals forces which form a denser and more tightly protective film, which drastically decreases the steel surface corrosion. Furthermore, FB-MAL, molecules may work as a bridge for the approaching Ni^{2+} to reach the C-steel surface from the aggressive media. Consequently, Ni^{2+} and the FB-MAL molecules exhibit a strong synergistic inhibition effect for C-steel in 2 M HCl.

The proposed mechanism was confirmed as described in the next sections.

3.5.1 Scanning electron microscopy (SEM). Fig. 9 shows SEM micrographs of C-steel immersed for 6 h in free 2 M HCl (a), 2 M HCl containing 600 ppm of FB-MAL (b), and 2 M HCl containing 600 ppm of FB-MAL + 100 ppm of Ni^{2+} (c).

The morphology in Fig. 9a shows a rough surface, which characterizes the uniform corrosion of C-steel in acid solution. In the presence of FB-MAL, Fig. 9b, a slightly smooth surface can be observed because of the formation of the green inhibitor's protective film on the metal surface. However, the presence of 100 ppm Ni^{2+} together with the FB-MAL efficiently enhances the surface smoothness of the C-steel surface (Fig. 9c). This finding may confirm the synergism between the Ni^{2+} and the FB-MAL molecules for improving the efficiency of inhibition for the C-steel.

3.5.2 FT-IR spectra studies. The differentiation of the FT-IR spectra of both FB-MAL and the adsorption product of the scratched samples of the C-steel surface in the systems studied are shown in Fig. 10. There are considerable changes in the FT-IR absorption bands for different groups of FB-MAL molecules after the weight loss test. A broad and strong peak for the –OH stretching band of alcohol or phenol, which was related to FB-MAL, and centered at 3419 cm^{-1} shifted to 3442 and 3441.24 cm^{-1} with and without 100 ppm of Ni^{2+}, respectively. The peak at 2935 cm^{-1} corresponding to the –C–H aromatic stretching frequency changed to the absorption peaks at 2924 cm^{-1} with and without Ni^{2+}. The sharp peak of the FB-MAL which estimated the –C=C– vibrations in the aromatic ring, alkenes and/or –C=O– (ref. 37 and 38) at 1633 cm^{-1} became a poor absorption peak and changed to weak absorption bands at 1670 and 1635 cm^{-1} with and without 100 ppm Ni^{2+}, respectively. Also the sharp peak at 1412 cm^{-1} for the FB-MAL estimated to be the $-CH_2$ bending frequency, was converted to poor absorption peaks at 1384 cm^{-1} for the two inhibitor systems studied. The band appearing at 1256 cm^{-1} for the FB-MAL

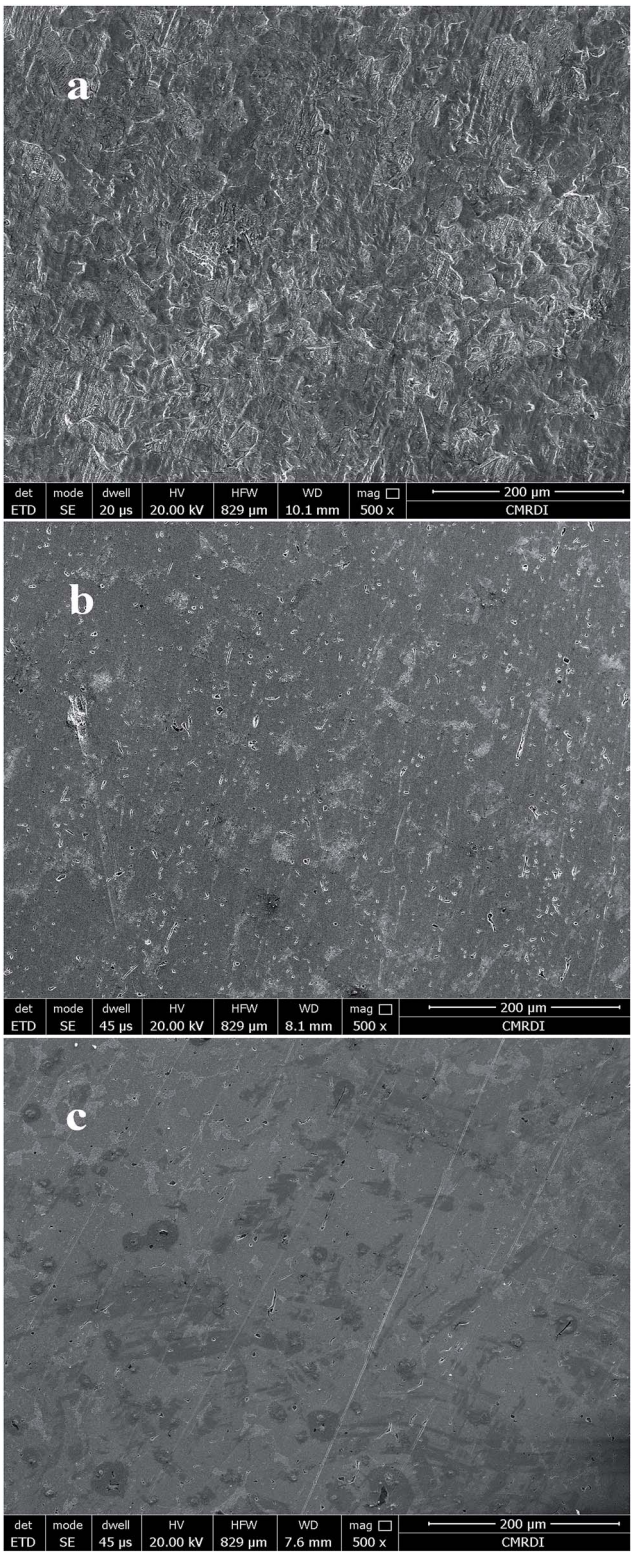

Fig. 9 SEM images of C-steel immersed in 2 M HCl (a) free, (b) containing 600 ppm of FB-MAL, (c) containing 600 ppm of FB-MAL + 100 ppm Ni^{2+}.

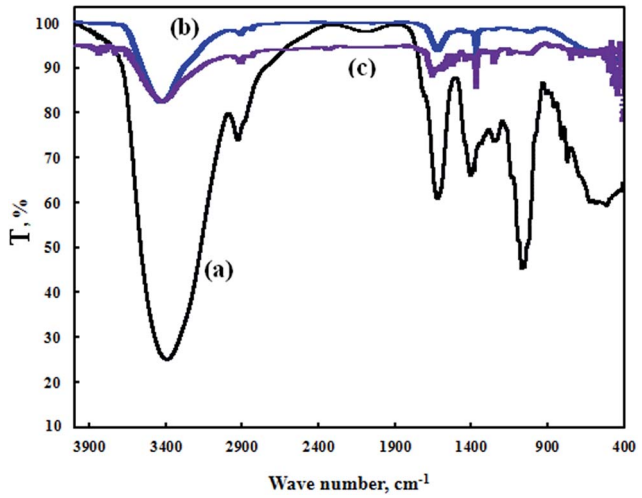

Fig. 10 FT-IR spectra of (a) crude FB-MAL, (b) adsorbed layer formed on the C-steel surface after immersion in 2 M HCl containing 600 ppm of FB-MAL, and (c) adsorbed layer formed on the C-steel surface after immersion in 2 M HCl containing 600 ppm of FB-MAL + 100 ppm Ni^{2+}.

which corresponds to the vibrations of the aromatic ring had nearly disappeared after the weight loss tests. The band of FB-MAL at 1079 cm^{-1} which was assigned to the –C–O stretching vibration (alcohol/ester) became negligible in the scratched samples as shown in Fig. 10. The current changes in absorption bands show the adsorption of different components of the FB-MAL at the C-steel surface with and without Ni^{2+}.

3.5.3 UV-Visible absorbance studies. UV-Visible spectroscopy gives the strongest evidence for the formation of metal–inhibitor complexes. UV-Visible absorption spectra obtained from 2 M HCl solution containing 50 ppm FB-MAL before and after the corrosion weight loss tests of C-steel with and without Ni^{2+} cations are shown in Fig. 11. From careful inspection of the UV-Vis spectra obtained, those of FB-MAL exhibiting two absorption maxima at about 224 nm and 338 nm before immersion of the C-steel coupon can be observed. The first band can be attributed to π–π* transition whereas the second band refers to the n–π* transition.[39,40] After the weight loss tests in 2 M HCl solution containing 50 ppm of FB-MAL had been conducted on the C-steel sample for 6 h, the two maxima absorption peaks shifted to 228 nm and 340 nm, respectively. Furthermore the presence of synergistic Ni^{2+} in the tested solutions exhibits two absorption maxima at about 228 nm and 342 nm. Such changes in both, the position of the absorption maxima and the absorbance values indicates the complex formation between the present species in solution. However, there is no change in the shape of the absorption spectra. These experimental findings emphasize the formation of the complex between Fe^{2+} and FB-MAL molecules with and without Ni^{2+}.[33]

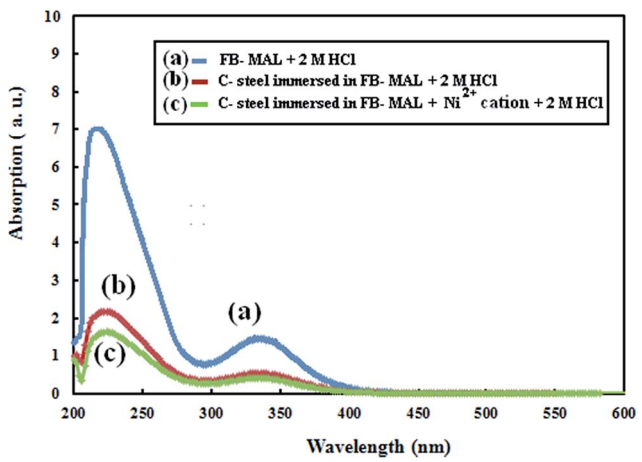

Fig. 11 UV-Visible spectra of the FB-MAL + 2 M HCl before and after the C-steel immersion with and without Ni^{2+} cations.

4. Conclusions

This research has led to the following conclusions:

(1) FB-MAL acts as a good, eco-friendly green inhibitor for the corrosion control of C-steel in 2 M HCl solution.

(2) FB-MAL acts as a mixed inhibitor by inhibiting both cathodic and anodic reactions and the adsorption of FB-MAL at the surface of C-steel follows Langmuir adsorption isotherm.

(3) The inhibitive performance of the novel FB-MAL is improved by a combination of different concentrations of FB-MAL with 100 ppm of Ni^{2+}.

(4) The IE obtained from the weight loss, potentiodynamic, and EIS measurements, were all in good agreement.

(5) Results from SEM, FT-IR and UV-Vis spectroscopy show that, the addition of inhibitors to aggressive solutions results in the formation of a protective film at the C-steel surface.

Acknowledgements

The authors wish to thank all the staff members at the Chemistry Department, Benha University, and the Central Metallurgical R&D Institute, Egypt for their guidance. The authors are greatly thankful to Cairo Oil Refining Company for petroleum refining, and for providing the C-steel coupons.

References

1 G. Moretti, F. Guidi and F. Fabris, *Corros. Sci.*, 2013, **76**, 206–218.
2 M. S. Al-Otaibi, A. M. Al-Mayouf, M. Khan, A. A. Mousa, S. A. Al-Mazroa and H. Z. Alkhathlan, *Arabian J. Chem.*, 2014, **7**, 340.
3 A. Khamis, M. M. Saleh and M. I. Awad, *Corros. Sci.*, 2013, **66**, 343–349.
4 M. A. Hegazy and S. A. El-Tabei, *J. Surfactants Deterg.*, 2013, **16**, 221–232.
5 D. Kesavan, M. Gopiraman and N. Sulochana, *Chem. Sci. Rev. Lett.*, 2012, **1**, 1.
6 K. Boumhara, M. Tabyaoui, C. Jama and F. Bentiss, *J. Ind. Eng. Chem.*, 2015, **29**, 146–155.
7 K. S. Beenakumari, *Green Chem. Lett. Rev.*, 2011, **4**(2), 117–120.
8 A. Saviour Umoren, B. Ime Obot and M. Zuhair Gasem, *Ionics*, 2015, **21**, 1171–1186.

9 A. Torresa Rodríguez, M. G. Cisnerosb Valladares and J. G. Rodríguez González, *Green Chem. Lett. Rev.*, 2016, **9**(3), 143–155.
10 K. Krishnaveni, J. Ravichandran and A. Selvaraj, *Ionics*, 2014, **20**, 115–126.
11 M. Shabani-Nooshabadi and M. S. Ghandchi, *Metall. Mater. Trans. A*, 2015, **46**, 5139.
12 D. Kumar Verma and F. Khan, *Green Chem. Lett. Rev.*, 2016, **9**(1), 52–60.
13 A. Y. El-Etre and A. I. Ali, *Chin. J. Chem. Eng.*, 2017, **25**, 373–380.
14 T. Balakrishnan, S. Sathiyanarayanan and S. Mayavan, *ACS Appl. Mater. Interfaces*, 2015, **7**, 19781.
15 G. Chiffelle Italo, F. Huerta Amanda and R. Lizana Diego, *Chilean Journal of Agricultural Research*, 2009, **69**, 138.
16 L. He, N. Yin, J. W. Cheng, X. Q. Wu, J. X. Jiang and X. L. Song, *Fitoterapia*, 2009, **80**, 399.
17 A. Hadjiakhoondi, H. Vatandoostb, M. Khanavia, H. Reza Sadeghipour-Roodsaric, M. Vosoughid, M. Kazemia and M. R. Abaib, *Iran. J. Pharm. Sci.*, 2006, **2**(2), 97–102.
18 M. A. Amin, H. Shokry and E. M. Mabrouk, *Corrosion*, 2012, **68**(8), 699–712.
19 M. Abdallah, E. M. Kamar, A. Y. El-Etre and S. Eid, *Prot. Met. Phys. Chem. Surf.*, 2016, **52**(1), 140–148.
20 M. Salah Tawfik, *RSC Adv.*, 2015, **5**, 104535–104550.
21 M. M. R. Ali, C. M. Mustafa and M. Habib, *J. Sci. Res.*, 2009, **1**(1), 82–91.
22 E. C. Potter, *Electrochemist Principle and Applications*, Britain, 1976.
23 R. S. Thornhill, *Ind. Eng. Chem.*, 1945, **37**(8), 706–708.
24 K. J. Vetter, *Electrochemical Kinetics*, Academic Press, New York, 1962.
25 *Science Data Book*, ed. R. M. Tennet, Oliver and Boyd, Edinburgh, 1978, vol. 56, p. 478.
26 M. Hosseini, S. F. L. Mertens and M. R. Arshadi, *Corros. Sci.*, 2003, **45**, 1473.
27 H. B. Rudresh and S. M. Mayanna, *J. Electrochem. Soc.*, 1977, **124**, 340.
28 A. J. Bard and L. R. Faulkner, *Electrochemical Methods*, John Wiley & Sons, New York, 1980, p. 517.
29 A. S. Fouda, H. Tawfik, N. M. Abdallah and A. M. Ahmd, *Int. J. Electrochem. Sci.*, 2013, **8**, 3390–3405.
30 S. Ramazan, *Corros. Sci.*, 2010, **52**, 3321–3330.
31 N. A. Negma, N. G. Kandile, E. A. Badr and M. A. Mohammed, *Corros. Sci.*, 2012, **65**, 94.
32 A. Doner and G. N. Kardas, *Corros. Sci.*, 2011, **53**, 4223.
33 R. Solmaz, E. Altunbas and G. Kardas, *Mater. Chem. Phys.*, 2011, **125**, 796.
34 R. Solmaz, G. Kardas, M. Culha, B. Yazıcı and M. Erbil, *Electrochim. Acta*, 2008, **53**, 5941–5952.
35 F. Suedile, F. Robert, C. Roos and M. Lebrini, *Electrochim. Acta*, 2014, **133**, 631–638.
36 R. Solmaz, *Corros. Sci.*, 2014, **79**, 169.
37 W. Kemp, *Organic Spectroscopy*, Palgrave, New York, 3rd edn, 2009, pp. 58–88.
38 T. Ramde, S. Rossi and C. Zanella, *Appl. Surf. Sci.*, 2014, **307**, 209–216.
39 M. Badertscher, P. Bühlmann and E. Pretsch, *Structure Determination of Organic Compounds*, Springer, Fourth, Revised and Enlarged Edition, 2009.
40 R. Parthik, P. Muthukrishnan, C. Shen-Ming, B. Jeyaprabha and P. Prakash, *Int. J. Electrochem. Sci.*, 2015, **10**, 3707–3725.

